FINAL REPORT

# STUDIES OF REACTION GEOMETRY IN OXIDATION AND REDUCTION OF THE ALKALINE SILVER ELECTRODE

J. P. L. 951554

This work was performed for the Jet Propulsion Laboratory, California Institute of Technology, sponsored by the National Aeronautics and Space Administration under Contract NAS7-100.

Eliot A. Butler

Angus U. Blackham

Department of Chemistry

Brigham Young University

Provo, Utah

April 10, 1967

# ABSTRACT

A double-Luggin capillary method has been used to measure potential variations in the vicinity of a working silver electrode. Current and potential distributions around several simple electrode configurations have been determined. These results can be extended to predict current density and potential variations around other electrode configurations. Equipotential maps are presented for several working electrodes. A comparison of experimental results from this study with a theoretical study on current distribution is made.

A method for estimation of effective electrolytic surface area has been developed. The method is based upon the assumption of constant depth of the $Ag \rightarrow Ag_2O$ oxidation of a silver electrode at fixed current density. A method for preparing a standard electrode surface which has area reproducible to $\pm 3\%$ is reported. Data are presented to show a reproducibility of $\pm 10\%$ in surface area estimations of sintered silver electrodes.

Our observations indicate the presence of an organic residue on commercial sintered silver electrodes part of which is hydrocarbon in character and part of which is carbonaceous. This appears to explain the earlier observation that microscopic portions of some sintered silver electrodes are unreactive.

# OBJECTIVES

The objectives of this contract are

(1) To characterize current and potential variations in the vicinity of a silver electrode during electrolysis as functions of cell and electrode geometry and of state of charge.

(2) To develop a method for the measurement of effective electrolytic surface area of a silver electrode.

(3) To characterize non-silver residues in sintered electrodes.

# SECTION I

## POTENTIAL VARIATION OVER THE ELECTRODE SURFACE

The chemical reactions that occur at the surface of a working electrode do not occur uniformly over the surface. Edges, corners, and points of stress of an electrode show differences from the smooth portion of the electrodes. A knowledge of current and potential variations in the regions of electrolyte near a working electrode should help one to predict the differences in reaction over the electrode surface.

### Appartus and Reagents

A cell was designed and built with two Luggin capillaries mounted on micrometer drives to permit simultaneous measurement of the difference in potential ($\Delta\phi$) existing between any two points around a working electrode. One of the capillaries was controlled by two micrometer drives mounted at right angles to each other permitting movement in two dimensions. The position of the capillaries was thus controlled to $\pm$. 001 inch. (See Figure 1)

The capillaries were made from 3 mm. soft glass tubing with Intramedic polyethylene tubing (O. D. .024", I. D. .011") sealed into a constricted end with epoxy cement. The seal was tested for air tightness, water tightness, and electrical leakage.

The measuring circuit consisted of two separate mercury-mercuric oxide reference electrodes connected by electrolyte (0.1 N KOH) through the two capillaries. Two ungreased ground-glass stopcocks placed in the rubber tubing connection between the capillaries and the reference cells prevented electrolyte flow from the test cell to the reference cells. Electrical connection was made by forcing electrolyte under pressure through the tubing and stopcocks, and wetting the ground stopcock surfaces before closing them. The $\Delta\phi$ measurements were made with a Leeds and Northrup K-3 potentiometer

or were recorded with a Leeds and Northrup Speedomax H recorder. For some experiments a simultaneous potential-time curve was recorded on a Varian recorder.

The sample electrodes are constructed from 99.99% pure silver foil 0.011 cm. thick or of Yardney sintered silver plates 0.038 cm. thick. Lacquer was used to coat parts of the electrodes as shown in Figures 6a, 7a, and 9a. The counter electrode used was a platinum foil 2 x 2 cm. or a 1.8 mm. platinum sphere. A rectangular trough (4.5 x 4.5 x 10.3 cm.) with the silver foil test electrode covering completely one end and the platinum foil counter electrode covering the other end, similar in design to a Haring[1] cell, except for the two gauze electrodes, was also constructed.

A 180 volt battery in series with resistors of appropriate sizes supplied the lower currents used. Constant currents above 8 ma. were provided by a Hewlett-Packard Model 881A power supply.

An ammoniacal electrolyte was made from 14.7 N $NH_4OH$ reagent to which 0.1 mole $KNO_3$ was added per liter to improve conductivity. The 0.1 N KOH was made from KOH reagent with precautions taken to prevent $CO_2$ contamination.

## Potential Distribution Experiments

Experimental. A number of experiments was performed in order to determine the causes of the $\Delta\phi$ or potential difference occurring on the test electrodes. The results indicate that there are at least two different phenomena involved. The first is an uneven current distribution caused by the geometry of the cell and the electrode. The second is an unequal oxidation of the electrode where one portion of the electrode is farther along the potential-time curve than are other portions. Two different electrolytes were used in the investigations: 0.1 N KOH and 14.7 N $NH_4OH$ with $KNO_3$ added to increase its conductivity. Unlike the KOH, the $NH_4OH$ electrolyte prevented the buildup

of oxide on the test anodes with the resulting potential changes. Thus the local potential, $\phi$, at any point is constant in the ammoniacal electrolyte. In the KOH electrolyte the local potential changes with the electrode potential because of oxide build-up and the resulting change in reaction, i.e., the change from $Ag \rightarrow Ag_2O$ to $Ag_2O \rightarrow AgO$.

1. Experiments in ammoniacal electrolyte.

No $\Delta\phi$ was measured between the edge and center on the silver anode in the Haring cell. This result agrees with earlier work[1, 2] which indicates a uniform current and potential distribution in the Haring cell. If the platinum foil counter electrode covering the end of the Haring cell is replaced with the 1.8 mm. platinum sphere counter electrode, the potential is found to be more anodic on the portion of the silver anode nearest the platinum sphere counter electrode.

A number of suspended foil electrodes has been tested in the ammoniacal electrolyte and all show potentials more anodic at the edge. Equipotential maps (Figures4-9) for several electrode configurations were made while the electrodes were undergoing oxidation in the ammoniacal electrolyte. These also show a higher potential at the edge than at the center.

2. Experiments in 0.1 N KOH electrolyte.

$\Delta\phi$ values were measureable between the edge and center on the silver anode in the Haring cell filled with KOH. This was not expected in view of the experiments in the ammoniacal electrolyte which showed a uniform current and potential distribution in the Haring cell. These $\Delta\phi$ values were recorded during both oxidation and reduction of the silver electrode. Two peaks occurred in the resulting $\Delta\phi$ curve during oxidation and two peaks occurred during reduction. Because the peaks appeared to correspond with changes in the state of oxidation of the electrode, simultaneous $\Delta\phi$, potential (relative to mercury-mercuric oxide reference), and differential of potential curves were recorded. A third mercury-mercuric oxide reference electrode was used for measurement of the potential of the silver electrode. The differential of the potential-time curve was obtained with an operational amplifier differentiator. (Figure 1a).

The simultaneous curves (Figure 2, curves A, B and D) show how the $\Delta\phi$ peaks correspond with changes in the reaction potential.

Similar curves were found for the $\Delta\phi$ between the edge and center of electrodes suspended in the KOH electrolyte. In addition to the peaks which occurred at the time of change of reaction, an initial $\Delta\phi$ was noted which can be attributed to the non-uniform current distribution around the suspended electrodes. (Figure 2, curves A, B, C)

Experiments were performed in a Haring cell in which the platinum foil counter electrode had been replaced by the small platinum sphere counter electrode. The electrolyte was 0.1 N KOH. When the counter electrode was placed within 2 cm. of the silver electrode and current densities of the order of 10 ma/cm$^2$ were used, a reaction such as the formation of AgO or the evolution of oxygen was observed to begin at the center and then spread out to the edges of the electrode. The extremely high current density in the regions near the small platinum sphere and the large potential gradients which result help account for this. This observation also suggests the possibility of gas formation in regions of an electrolytic cell where because of geometry a very high current density exists.

Discussion. For the experiments done in ammoniacal electrolyte, geometrical arguments, which indicate a greater number of current paths available for the edge of an electrode as compared to the center, account for the greater current density and potential existing at the edge.

An extension of arguments made by Wagner[3] about current distribution in the electrolytic cell explains the shape of the equipotential lines (Figures 4-9) found for the six silver electrodes in the ammoniacal electrolyte. Similar arguments by others[1, 2] also predict that no potential differences should exist on the silver anode in the Haring cell filled with the ammoniacal electrolyte, because of the uniform current distribution in that cell. When this cell is altered by replacing the platinum foil counter electrode with a small platinum sphere, the current density is at a maximum on those regions of the

silver electrode which are nearest the sphere.

All of these observations appear to follow from the unequal current distribution caused by the geometry of the electrodes and the cell. This phenomenon has been observed by other workers[4, 5]. Our results in the ammonia solution are in agreement with existing theory and can be predicted by arguments based on the geometry of the electrodes and the cell.

A somewhat more complex model must be considered when discussing the results obtained in the 0.1 N KOH electrolyte. In addition to geometry effects there is an unequal oxidation of the electrode where one portion of the electrode is farther along the potential-time curve than are other portions. This phenomenon seems to be of significant effect only at the time of a reaction change on the silver electrode (i.e., the change from $Ag \rightarrow Ag_2O$ to $Ag_2O \rightarrow AgO$ or from the latter to the formation of $O_2$) where the potential-time curve is especially steep.

This phenomenon is apparently not caused by large inequalities in the current distribution, for large peaks occurred (Figure 2 curve D) in the $\Delta\phi$ curve in the Haring cell using the 0.1 N KOH electrolyte. These peaks were associated with changes in the cell reaction and thus correspond to the steep portions of the potential-time curve. In each case the edge was found to be more anodic than the remainder of the electrode during oxidation of the silver.

Examination of the $\Delta\phi$ curves of the suspended electrode in 0.1 N KOH suggests that these curves are probably a combination of both unequal current distribution and unequal oxidation. Addition of curves D and E to form curve C in Figure 3 illustrates this.

Booman and Holbrook[5] have shown that if a counter electrode is used which is small in size compared to the working electrode, the current density between them will be greater in the region near the small electrode. This was the result obtained with the 1.8 mm. platinum sphere counter electrode placed at distances less than 2 cm. from the larger working electrode. In 0.1 N KOH at high current

extreme variations in current density over its surface.

For the case where only one side of the electrode is available for reaction (Figure 6a) there is a difference in the equipotential lines near the edge from those in Figure 4 where both sides of the electrode can react. The greater number of current paths directed toward the edge of a suspended electrode when the reverse side is non-reactive accounts for this difference. In Figure 7 where these current paths around the reverse side are not available the equipotential patterns are much like those around the front side of the electrode in Figure 4.

Figures 8 and 9 showing potential distributions around an unreactive hole or spot on an electrode have essentially the same equipotential patterns. Again, consideration of the current paths available for each reaction site enables one to explain the current and potential distribution. The spot painted on the center of electrode 9a resembles a non-reactive spot in any working cell in its effect on potential and current distribution.

Micrometer measurements taken of the thickness of electrodes after extensive oxidation in the ammoniacal electrolyte show that a significantly greater amount of reaction has taken place at the edge than at the center. For example, center and edge measurements on a typical electrode were 0.17 mm. and 0.11 mm., respectively.

The spacing of the equipotential lines shows qualitatively the current distribution; the closer the spacing the greater the current density. From Ohm's law the current density, J, at any point is the product of the local potential gradient, $\frac{\partial \phi}{\partial n}$, and the electrical conductivity, $\sigma$:

$$J = \sigma \frac{\partial \phi}{\partial n} \qquad (1)$$

In this expression, n is the distance in the direction of current flow. Since J is a vector,

$$J = \sigma \left[\left(\frac{\partial \phi}{\partial x}\right)^2 + \left(\frac{\partial \phi}{\partial y}\right)^2 + \left(\frac{\partial \phi}{\partial z}\right)^2\right]^{1/2} \qquad (2)$$

where x, y, and z are the Cartesian coordinates indicated in Figure 10a.

Measurements of $\phi$ in two directions (x, y) were made using the micrometer drives which permitted capillary movement in two dimensions. Plots of $\phi$ versus x and of $\phi$ versus y were made. From these plots the values of $\partial\phi/\partial x$ and $\partial\phi/\partial y$ were obtained. Because we are able to evaluate only $\partial\phi/\partial x$ and $\partial\phi/\partial y$ with the present apparatus the vertical strip electrode shown in Figure 10 was chosen for analysis. Since this electrode extends from the solution surface to the bottom of the cell the current density distribution in the vertical z direction is assumed to be uniform and the potential gradient $\frac{\partial\phi}{\partial z}$ zero. J values were then calculated from equation (2) by use of the experimental $\partial\phi/\partial x$ and $\partial\phi/\partial y$ values and the measured value of $\sigma$ (0.00947 ohm$^{-1}$ cm$^{-1}$). A plot of $J/J_{ave.}$ is shown in Figure 11 ($J_{ave.}$ is the total current divided by the geometric area of the electrode).

Wagner[3], in his theoretical analysis considered an electrode very similar to our strip electrode in Figure 10. The electrode which Wagner analyzed was assumed to be in a cell of such size that both the width of the cell and the distance between anode and cathode were very large compared to the width of the working electrode. In our cell the distance separating the anode and cathode is about 10 times the width of the anode but the width of the cell is only slightly more than 3 times the anode width. This may account for some difference between his theoretical results and our experimental results.

Wagner's analysis is based on numerical or graphical solutions of an integral equation derived from Poisson's equation and Ohm's law. A plot of $J/J_{ave.}$ as calculated by Wagner is included in Figure 11.

Both Wagner's plot and our experimentally determined plot are based on a K/a ratio of 0.10. This ratio represents the variables which affect the current distribution in the cell. In this ratio, a is the half-width of the electrode. The dimensionless parameter, K, is the product of the electrical conductivity, $\sigma$, and the absolute

slope of the polarization curve for the cell.

$$K = \sigma \left| \partial E / \partial J \right|$$

The polarization curve was made by plotting the electrode potential as a function of several different current densities. (See Figure 12). Figure 12 is only that part of the polarization curve for the silver electrode in the region of current density used in our experiments. Because the slope of polarization curves is dependent on current density it is evident that a change in current density will cause a change in $J/J_{ave.}$, the distribution of current density.

There are several sources of error in our experiments. Because it is a working electrode there is an unavoidable change in $\sigma$ because of the build-up of reaction products and the consumption of electrolyte for the reaction in addition to loss of $NH_3$ and $H_2O$ by evaporation. Another problem is the inherent loss of precision in taking derivatives. In addition, Wagner's calculation is based on a cell with dimensions somewhat different from ours. To approach his cell dimensions we would need to use a very narrow electrode or a very large cell. In view of this, the agreement of the two plots in Figure 11 is good. Both plots show a high deviation from the average current density at the edge which decreases to near average current density a short distance from the edge as one approaches the center of the electrode. Thus it is only the edge region which shows marked deviation from average current density. Thickness measurements of electrodes which have undergone extensive oxidation in the ammoniacal electrolyte show this same pattern, with 3 or 4 times as much silver having been dissolved away from the edge of the electrode as from the center.

# SECTION II

## SURFACE AREA ESTIMATION

Sintered silver electrodes allow appreciably more charge per unit mass to be applied than do sheet silver electrodes. The choice of optimum charge and discharge rates for such electrodes is made simpler if the effective surface area is known. Allen established that the depth of penetration of an oxide layer may be determined coulometrically by measurement of the length of the potential plateau of that oxidation at constant current.[6] The following equation may be applied to the resulting data to find the depth of penetration expressed as the number of monolayers of penetration.

$$X = \frac{N_o}{F\left[\frac{N_o \rho}{M}\right]^{2/3}} \cdot \frac{It}{a} = kDt$$

where

- $X$ = number of monolayers of penetration
- $N_o$ = Avogadro's number
- $F$ = Faraday
- $\rho$ = density in $g/cm^3$
- $M$ = atomic weight (g/mole)
- $I$ = current (amps)
- $a$ = surface area ($cm^2$)
- $t$ = plateau length (minutes)
- $D$ = current density ($amps/cm^2$)
- $k$ = a constant

If the assumption is made that at a given current density, the depth of penetration, on the average, will be equal for smooth as well as for uneven surfaces, the following result is obtained:

Assume that if $D_1 = D_2$ then $X_1 = X_2$.

From the equation above $X_1 = kD_1t_1$ and $X_2 = kD_2t_2$.

Therefore $kD_1t_1 = kD_2t_2$ and $t_1 = t_2$

This means that if two electrodes have equal plateau lengths, they were oxidized at the same current density and have equal depths of penetration.

A standard curve of known current density versus plateau length (expressed in minutes) has been plotted. (See Table I and Figure 14). From this curve unknown surface areas have been determined. By changing the applied current until the plateau length matches a point on this standard curve a cross reference to the known current density can be obtained, and thus the unknown surface area may be determined.

Sample Calculation. A sintered silver electrode with an apparent or a geometrical area of 0.688 $cm^2$ is electrolyzed at a constant applied current of 4,000 μamp. The time equivalent of the length of the first potential plateau is 14.4 minutes (Figure 13). From the standard curve (Figure 14), a current density D = 91.0 μamp/$cm^2$ is noted for t = 14.4 minutes.

$$D_1 = D_2 = \frac{I_2}{a_2} = 91.0 \text{ μamp/cm}^2$$

$$a_2 = \frac{4,000 \text{ μamp}}{91.0 \text{ μamp/cm}^2} 2 = 44.0 \text{ cm}^2$$

The roughness factor is the calculated surface area divided by the geometrical area of the electrode.

$$\text{R. F.} = \frac{44.0 \text{ cm}^2}{0.688 \text{ cm}} 2 = 63.4$$

An indication of the magnitude of the surface which is perhaps more meaningful is given by the area per unit mass:

$$\frac{44.0 \text{ cm}^2}{0.093 \text{ g}} = 469 \text{ cm}^2 \text{/g}$$

Another representation of the surface is given by the area per unit volume:

$$\frac{44.0 \text{ cm}^2}{0.16 \text{ cm}^3} = 273 \text{ cm}^{-1}$$

The Standard Curve. The silver electrodes which provided the data for the construction of the standard curve, Figure 14, were prepared from glass discs of 18 mm. diameter (2.54 $cm^2$ surface area) which have had a silver film deposited upon them by vacuum

densities (10 ma/cm$^2$) it was also possible to see a reaction such as the evolution of oxygen begin first in the area on the silver electrode nearest the platinum sphere and then expand radially over the remainder of the electrode. An attempt was made to measure the $\Delta\phi$ between the center and edge under these conditions where there was visible evidence for large potential differences. The largest $\Delta\phi$ of 400 mv. was measured during the reduction reaction where free silver was seen in the center portion of the electrode under one measuring capillary while the yet unreduced silver oxide was seen covering the edge area under the second measuring capillary. The $\Delta\phi$ curve rose toward the 400 mv. peak as the border between the free silver and the silver oxide moved out in a circle of increasing radius and attained its highest value just before the border crossed beneath the second capillary tip.

## Potential Mapping and Current Distribution

A series of $\Delta\phi$ measurements was made around each of several electrodes (Figures 4a - 9a) in the ammoniacal electrolyte.

Ammonia prevents, by the formation of silver ammine complexes, the build-up of $Ag_2O$ on the electrode and the reaction and potential change which follows that build-up. Thus if we neglect conductivity changes caused by the concentration build-up of reaction products, the $\Delta\phi$ between two points in the solution is constant with time.

All measurements were made with one capillary fixed in the center which was arbitrarily assigned the value of zero. From these measurements equipotential lines (20 mv. apart) were constructed. (Figures 4-9)

Comparison of Figures 4 and 5 for the solid and sintered electrodes indicates the same general potential variation. Near the edge of the sintered electrode the equipotentials are separated somewhat more than those near the edge of the solid electrode indicating a more moderate potential variation. This is probably caused by the much greater surface area of the sintered electrode which leads to less

vaporization. The main problem experienced with these standard electrodes has been the poor adhesion of the silver to the glass.[7] Without proper adhesion, the silver tends to dissolve off the discs during the oxidation run. This problem has been partially overcome by first cleaning the discs in soap and water and then in alcoholic potassium hydroxide solution. They are then rinsed in distilled water and wiped dry with lint-free tissue. The rubbing of the glass puts a static charge on the surface of the discs which appears to help the adhesion of the silver to the glass. With these discs the reproducibility of the plateau length is good within 3 to 7 per cent (See Table I).

X-ray studies of silver films produced by vacuum deposition indicate that the gross crystal structure produced is almost identical to that observed in sintered silver plates. Furthermore, the thicker the film deposited the more nearly the surface area of the film approaches the surface area of the glass substrate.[8] The films used in these experiments are on the order of 3,000 to 4,000 monolayers thick, and therefore their surface areas should approach the geometrical areas of the glass discs to well within our experimental limits.

Larger glass discs (22 mm. diameter; 3.80 $cm^2$ area) were prepared in the same manner as the standard electrodes. These discs were then oxidized and the plateau length matched with the standard curve. The experimental surface area agreed to within 3 per cent of the geometric area in the regions of greatest curvature of the plot (Figure 14). The current densities used ranged from 100 to 300 $\mu amp/cm^2$.

To avoid effects of cell geometry upon the oxidation plateau length, we used a cylindrical platinum counter electrode. This gives the most uniform current distribution around the working electrode and is easy to reproduce. Also, the reaction cell has been thermostatted to $20 \pm .1^{\circ}C$ for reasons discussed later. See Figure 15 for a diagram of the apparatus.

Extension of Method to Silver Foil and Wire. A difference in the depth of oxidation might be expected in ordinary rolled silver foil as compared with these vapor deposited films because of a difference in the number of lattice imperfections per unit volume. The experimental evidence, however, indicates that the depth of oxidation is the same in rolled silver foil as in the vapor deposited silver. The reason for this conclusion is our observation that the roughness factor for the rolled silver foil is 1.3 and this is the same value for nickel foil obtained by double-layer capacitance measurements.[9]

Silver wire gave roughness factors closer to 1.00 than did the silver foil indicating less surface imperfections in the wire.

Extension of Method to Sintered Silver. Two commercial sintered silver electrodes are compared as determinations 4 and 5 of Table II. The Delco-Remy electrode gives values for roughness factors slightly higher than the Yardney electrode. The measurements for these electrodes were extended over a greater range of current densities and are shown in Figure 13.

Much higher currents were used because of the increased surface area of these sintered electrodes. The roughness factors (the electrolytic surface area divided by the geometric area) of 59 and 63 reported in Table II were determined in the region of smaller current flow. At high values of the applied current the roughness factors became smaller. (See Figure 13). The variation of these roughness factors as a function of applied current is not unreasonable, for, as the reaction is forced to go faster, any internal shielding or electrolyte depletion would become more evident and thus affect the extent of the total reaction. This could tend to cut down the effective electrolytic surface.

Effect of Temperature. Studies of the temperature effect upon the oxidation (See Figure 16) indicate that the extent of the reaction is dependent upon the temperature. The data in the figure were obtained

on sintered silver electrodes of constant size with the same total current used in each case. The change in plateau length from $0^{\circ}C$ to $50^{\circ}C$ is more than 7 fold. The change in conductivity of the solution is less than 3 fold over the same temperature range. Either or both of two effects could contribute to the significant change of oxidation plateau length with temperature:

1. It has been suggested that migration of ions in the oxide account for charge conduction between the metal and the electrolyte.[10] This migration would be expected to be very temperature dependent.

2. Changes in viscosity of the electrolyte with temperature may affect the extent of penetration of the electrolyte with the pores of the sintered electrode. Thus, the more viscous electrolyte would give the shortest plateau length because there would be less silver surface in contact with the electrolyte.

Conclusion. In the use of this method for estimation of electrolytic surface areas certain external variables must be controlled. These include temperature, electrolyte, and cell geometry. The most satisfactory current densities are those located in the range of greatest curvature on the plot of current density vs plateau length. In this "middle range" of the graph the effective surface area as calculated is almost constant.

On the upper part of the graph large changes in current density correspond to small changes in plateau length. Two reasons are suggested to account for the decreases in the effective electrolytic surface areas for these large current densities: (1) the rate of penetration of the surface by oxide may lag behind the rate of charge passing through the surface; (2) the rate of depletion of ions near the surface may be greater than the rate of diffusion of ions to the surface.

On the lower part of the graph small changes in current density correspond to large changes in plateau length. Dissolving of the argentous oxide from electrode may contribute to the poor results in this region since the rate of oxidation is so low.[11]

# SECTION III

## ORGANIC RESIDUES IN SINTERED SILVER ELECTRODES

Evidence was presented in the first quarterly report of J. P. L. Contract 951157 that commercial sintered silver electrodes may contain organic residues resulting from incomplete removal of organic binders during the sintering process. This evidence was the observation that the sintered silver electrodes after oxidation showed regions visible with a microscope where no oxidation had occurred.

In the catalytic oxidation of ethylene by silver with limited oxygen, Twigg [12] has observed the formation of a non-volatile deposit on the surface of the silver catalyst.

Our approach to the determination of the nature and amount of the residue on sintered silver electrodes has been pyrolysis of samples of electrodes in helium, hydrogen and oxygen and analyses of the products by gas chromatography and infrared spectrophotometry.

Apparatus. A Perkin Elmer Vapor Fractometer Model 154 D with a Leeds and Northrup Speedomax G recorder was used for the gas chromatographic analyses. Three columns were used with this instrument:

(1) A silica gel column, 4 ft;

(2) A molecular sieve column, 4 ft;

(3) A column of di-n-decylphthalate on firebrick, 3 ft. The infrared determinations were made with a Beckman IR 7 instrument.

A borosilicate glass pyrolysis chamber was constructed. A schematic diagram of this chamber is shown in Figure 17. It is fitted with a by-pass path so that the sample may be heated for a period of time such as five minutes in a tube furnace and then the gases swept into the main stream of the carrier gas for analysis.

Analyses. The amounts of gaseous products have been quite small. Therefore the assignment of the peaks in the gas chromatograms have

been made by comparison with retention times of known compounds suspected of being present in the samples. Sufficient amounts of products were obtained in some experiments to confirm the assignments of carbon dioxide, methane, and ethylene. The characteristic infrared absorption at 2350 $cm^{-1}$ was observed for carbon dioxide, at 1300 $cm^{-1}$ for methane and at 949 $cm^{-1}$ for ethylene. The molecular sieve column separates methane, carbon monoxide, oxygen, nitrogen. The silica gel column separates ethane, ethylene, and carbon dioxide; the four gases above have about the same retention time and are eluted together. The phthalate ester column separates carbon dioxide and water; all of the other gases discussed above are eluted together. Therefore we have used these three columns to analyze for six products: $CH_4$, CO, $C_2H_6$, $C_2H_4$, $CO_2$ and $H_2O$.

Carrier Gases. The silver samples were pyrolyzed in either helium, hydrogen, or oxygen. The gas chromatographic analysis was then made with the same gas as the carrier. Two different cylinders of helium were used. Helium of a technical or commercial grade apparently contained sufficient impurities to cause some chemical reactions. The methane, ethylene, and ethane observed as reaction products when this helium was used were probably formed as the residue on the electrode sample reacted with the hydrogen impurity.

A cylinder of helium labeled "ultra high purity" was obtained from the Matheson Company. Using this helium as the carrier gas we did not observe ethane and ethylene.

The analysis of this ultra pure helium is:

| | | | |
|---|---|---|---|
| $CO_2$ < | .05 ppm | $N_2$ | 4.2 ppm |
| $O_2$ | 0.9 ppm | Ar | 0.1 ppm |
| $H_2$ | 0.6 ppm | $CH_4$ | 0.0 |
| Ne | 10.1 ppm | $H_2O$ | 1.9 ppm |

In the presence of hydrogen as carrier gas hydrocarbons were produced. Carbon monoxide and carbon dioxide were also observed. We assume that the oxygen needed for the oxides was adsorbed on

the surface of the sintered silver before pyrolysis.

In the presence of oxygen as carrier gas, water and carbon dioxide are the principal reaction products. Water as a reaction product in the oxygen carrier indicates that some hydrogen is bonded to carbon in the residue.

Results. The results of the gas chromatographic analyses are summarized in Tables III and IV. Determinations 1 - 5 of Table III with technical grade helium show simple hydrocarbons and carbon oxides as products of pyrolysis. Determinations 6 and 7 with "ultra pure" helium show only carbon oxides. The interpretation for this change is that hydrogen as an impurity in the technical grade helium reacts with the carbonaceous residue to form hydrocarbons.

Determinations 8-12 of Table III with hydrogen show the same products as determinations 1 - 5 with technical grade helium. The carbon monoxide-carbon dioxide ratio is high in the hydrogen carrier.

Determinations 13-15 of Table III and 2-6 of Table IV resulting from the pyrolysis of three different commercial sintered silver electrodes in oxygen show quantities of carbon dioxide approaching one milligram $CO_2$ pyrolyzed from one gram of sintered silver.

Determinations 2-6 of Table IV also show water as a product of pyrolysis in oxygen. However, determination 1 of Table IV shows quantities of water of the same magnitude from pyrolysis in technical grade helium. An obvious interpretation is the adsorption of water on the sintered silver which is expelled in part at 250°C and more at 500°C. However, as the technical helium also contains oxygen as an impurity the water may result from reaction with hydrogen from the residue or hydrogen in the technical helium. Determination 2 of Table IV shows $CO_2$ and $H_2O$ from pyrolysis in technical helium. The same sample is then pyrolyzed in oxygen with 420 micrograms $CO_2$ and 90 micrograms $H_2O$ as products.

Determination 7 involves a sequence of successive runs with increasing temperature. Ultra pure helium was used. Small quantities

of carbon dioxide and water were released with each rise in temperature. The amounts at 350°C (10 μg. $CO_2$ and 18 μg. $H_2O$) are greater than the amounts at 410°C (5 μg. $CO_2$ and 4 μg. $H_2O$). This suggests that below ≈ 400°C any adsorbed $CO_2$ and $H_2O$ is released and above ≈ 400°C the residue reacts with adsorbed oxygen or with the oxygen (0.9 ppm) in the ultra pure helium carrier. The run 7(f) in oxygen shows 100 μg. $CO_2$ and 21 μg. $H_2O$. Our interpretation is that the carbon and hydrogen in these products can only come from a residue on the sintered silver.

Determinations 8 and 9 of Table IV show results of an attempt to make several runs in helium before the final run in oxygen at 600°. We were surprised at the low values for $CO_2$ and $H_2O$ (8(k)-28 μg., 9 μg; 9(k)-25 μg., 32 μg.) after pyrolysis in oxygen. Our interpretation is that during the ten repetitive runs in helium (8a-j and 9a-j) some of the carbon was lost as carbon monoxide. Evidence for this is taken from determinations 6 and 7 of Table III in which 30 μg. CO is observed along with 24 μg. $CO_2$.

Electrolytic oxidation of pyrolyzed electrodes. In Figure 18 a comparison is made of the electrolytic oxidation of three sintered silver electrodes. Curve A is typical of the $Ag \rightarrow Ag_2O$ oxidation. Curve B shows a similar oxidation but after the sintered silver electrode had been pyrolyzed in oxygen at 410°. Two differences are noted. Through the first part of curve B there is no region where the slope becomes negative as is typical of the regular electrodes. Also, the length of the plateau is slightly increased in curve B (9.55 ± 0.10 minutes based on three determinations compared to 9.15 minutes for the longest of several unpyrolyzed samples).

Curve C is similar in shape to curve B (no negative slope at the beginning of the plateau) but the length of the plateau is less (7.35 minutes). The electrode in this case had been pyrolyzed at 625°C. The decrease in plateau length probably reflects a decrease in effective electrolytic surface area caused by fusion or coalescence of sintered silver at the high temperature.

These observations suggest pyrolysis of sintered silver electrodes in oxygen as a means of removing surface impurities which may be reducing the efficiency of the electrodes and which are not removed by conventional cleaning procedures.

Conclusion. While our results do not permit a precise quantitative interpretation of the nature of the residue on sintered silver electrodes the presence of a residue partly hydrocarbon in character and partly carbonaceous in character is indicated. The results from pyrolyses in oxygen indicate approximately 400-500 μg. $CO_2$ and 100 μg. $H_2O$ from a 1.0 gram sample of sintered silver. This is approximately 10 micromoles $CO_2$ and 5 micromoles $H_2O$ or 1 atom C and 1 atom H for 1000 atoms of silver. Aromatic hydrocarbon residues may have a C-H atom ratio of approximately one. Equal amounts of a polymethylene residue [ $(CH_2)_n$ ] and a graphite type residue will give an average C-H atom ratio of approximately one.

From the observation by Fischer and Werner[13] that cyclononatriene forms a stable complex with silver nitrate through $\pi$ -olefin interaction

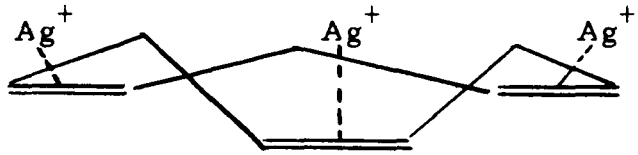


with silver ions one may expect that cyclic polyene residues are also possible on sintered silver electrodes.

## Future Work

Additional measurements of current and potential distribution over the electrode surface will be made for other K/a ratios. These data will permit a broader comparison with features of Wagner's theory.

Rates of oxidation and reduction of the alkaline silver electrode will be determined as a function of temperature, electrode geometry, and nature of the electrolyte. Consideration will be given to a mechanism consistent with these data.

The surface areas for sintered silver have been determined. To establish the usefulness of this method we need to measure surface areas of these electrodes by conventional methods. For example, a modification of the BET method based on a radioactive inert gas may be used.

The depth of penetration of oxidation of smooth silver plate is a function of current density and temperature. The irregularities of the surface of sintered silver may cause physical stresses not present on a smooth silver surface. Therefore electrolytic surface areas will be measured as a function of physical stresses on the electrode.

Pyrolysis of silver electrodes in oxygen as a means of cleaning will be given further study.

TABLE 1

Reproducibility of Oxidation Runs
Temperature 20°C

| Current Density ($\mu$ amp/cm$^2$) | Plateau Length (minutes) | Deviation |
|---|---|---|
| 97.9 | 13.5 | ± 2.9% |
| 101 | 11.1 | ± 3.2% |
| 158 | 6.2 | ± 2.4% |
| 236 | 3.2 | ± 4.3% |
| 355 | 1.85 | ± 2.9% |
| 590 | .85 | ± 6.6% |

TABLE 2

SURFACE AREA ESTIMATION

| Dtm | Type of Surface | Current ($\mu$ amp) | Surface Area Geometric $cm^2$ | Surface Area Experimental $cm^2$ | Roughness Factor | Area Per Unit Mass ($cm^2/g$) | Area Per Unit Volume ($cm^{-1}$) |
|---|---|---|---|---|---|---|---|
| | Silver deposited upon glass disc (22 mm, dia); | 603 | 3.80 | 3.76 | 0.99 | --- | --- |
| 1 | two current densities | 902 | 3.80 | 3.82 | 1.01 | --- | --- |
| | Unpolished silver foil cleaned with soap and | 602 | 2.54 | 3.30 | 1.30 | --- | --- |
| | water, varied area and | 602 | 2.54 | 2.79 | 1.10 | --- | --- |
| 2 | current density | 6300 | 19.60 | 21.67 | 1.10 | --- | --- |
| | Silver wire, cleaned | 910 | 5.00 | 5.14 | 1.05 | --- | --- |
| | with soap and water; | 910 | 5.00 | 5.23 | 1.06 | --- | --- |
| 3 | current density constant | 910 | 5.00 | 5.02 | 1.01 | --- | --- |
| | Delco-Remy sintered silver soaked in elec- | 3500 | .688 | 44.00 | 63.40 | 469 | 273 |
| | trolyte for 10 min; cur- | 3500 | .688 | 42.00 | 63.00 | 466 | 271 |
| 4 | rent density constant | 3500 | .688 | 43.60 | 63.20 | 468 | 272 |
| | Yardney sintered silver soaked in electrolyte | 3500 | .688 | 40.80 | 59.40 | 584 | 341 |
| | for 10 min; constant | 3500 | .688 | 40.40 | 59.10 | 581 | 339 |
| 5 | current density | 3500 | .688 | 40.60 | 59.20 | 582 | 339 |

Table III

Products from Pyrolyses of 1.0 gram Samples of

Sintered Silver Electrodes

| Dtm | Electrode | Carrier Gas | G.C. Column | Temp °C | Products in micrograms CO | $CH_4$ | $C_2H_6$ | $C_2H_4$ | $CO_2$ |
|---|---|---|---|---|---|---|---|---|---|
| 1 | Delco Remy | Helium-technical | Silica gel | 750° | 160* | | 2.2 | 0.9 | 130 |
| 2 | Ele. Storage Battery | Helium-technical | Silica gel | 750° | 40* | | 0.4 | 2.0 | 70 |
| 3 | Yardney | Helium-technical | Silica gel | 500° | 12* | | 2.3 | 4.5 | 35 |
| 4 | Delco Remy | Helium-technical | Silica gel | 500° | | | 4.4 | 17 | 59 |
| 5 ** | Delco Remy | Helium-technical | Silica gel | 750° | | | 0.6 | 21 | 4.9 |
| 6 | Delco Remy | Helium-ultra pure | Silica gel | 540° | | | 0 | 0 | 24 |
| 7 | Delco Remy | Helium-ultra pure | mol. sieve | 500° | 30 | 0 | | | |
| 8 | Delco Remy | Hydrogen | Silica gel | 650° | 13 | 25 | 9 | | 0.9 |
| 9 | Delco Remy | Hydrogen | Silica gel | 600° | 28 | | 1 | 2 | 9 |
| 10 | Delco Remy | Hydrogen | Silica gel | 650° | 29 | | 12 | 3 | 13 |
| 11 | Delco Remy | Hydrogen | mol. sieve | 650° | | 1.9 | | | |
| 12 | Delco Remy | Oxygen | Silica gel | 500° | | | 0 | 0 | 520 |
| 13 | Delco Remy | Oxygen | Silica gel | 500° | | | | | 510 |
| 14 | Ele. Storage Battery | Oxygen | Silica gel | 500° | | | | | 520 |
| 15 | Yardney | Oxygen | Silica gel | 500° | | | | | 870 |

* Value is for light gases which may include CO, $CH_4$, $N_2$, and $O_2$ which are not separated on this silica gel column.

** Pyrolysis made in a stainless steel tube.

Table IV

Products from Pyrolysis of 1.0 gram Samples of

Sintered Silver Electrodes

G.C. Column - n-decylphthalate on firebrick

| Dtm | Electrode | Carrier Gas | Temp °C | Products in micrograms $CO_2$ | $H_2O$ |
|---|---|---|---|---|---|
| 1.(a) | Delco Remy | Helium tech. | 250° | | 230 |
| 1.(b) | Delco Remy | Helium tech. | 500° | | 140 |
| 2.(a) | Delco Remy | Helium tech. | 500° | 65 | 88 |
| 2.(b) | Delco Remy | Oxygen | 500° | 420 | 90 |
| 3 | Delco Remy | Oxygen | 500° | 400 | 100 |
| 4 | Delco Remy | Oxygen | 500° | 470 | 100 |
| 5 | Elec. Storage Battery | Oxygen | 500° | 400 | 140 |
| 6 | Yardney | Oxygen | 500° | 560 | 160 |
| 7.(a) | Delco Remy | Helium ultra pure | 190° | 3 | 2 |
| 7.(b) | Delco Remy | Helium ultra pure | 240° | 4 | |
| 7.(c) | Delco Remy | Helium ultra pure | 350° | 10 | 18 |
| 7.(d) | Delco Remy | Helium ultra pure | 410° | 5 | 4 |
| 7.(e) | Delco Remy | Helium ultra pure | 525° | 11 | 16 |
| 7.(f) | Delco Remy | Oxygen | 525° | 100 | 21 |
| 7.(g) | Delco Remy | Oxygen | 525° | | 5 |
| 8.(a-e) | Delco Remy | Helium ultra pure | 400° | 18 | 9 |
| 8.(f-j) | Delco Remy | Helium ultra pure | 600° | 12 | 13 |
| 8.(k) | Delco Remy | Oxygen | 600° | 28 | 9 |
| 9.(a-e) | Elec. Storage Battery | Helium ultra pure | 400° | 14 | 4 |
| 9.(f-j) | Elec. Storage Battery | Helium ultra pure | 600° | 3 | 7 |
| 9.(k) | Elec. Storage Battery | Oxygen | 600° | 25 | 32 |

Figure 1 Diagram of test cell and measuring circuit

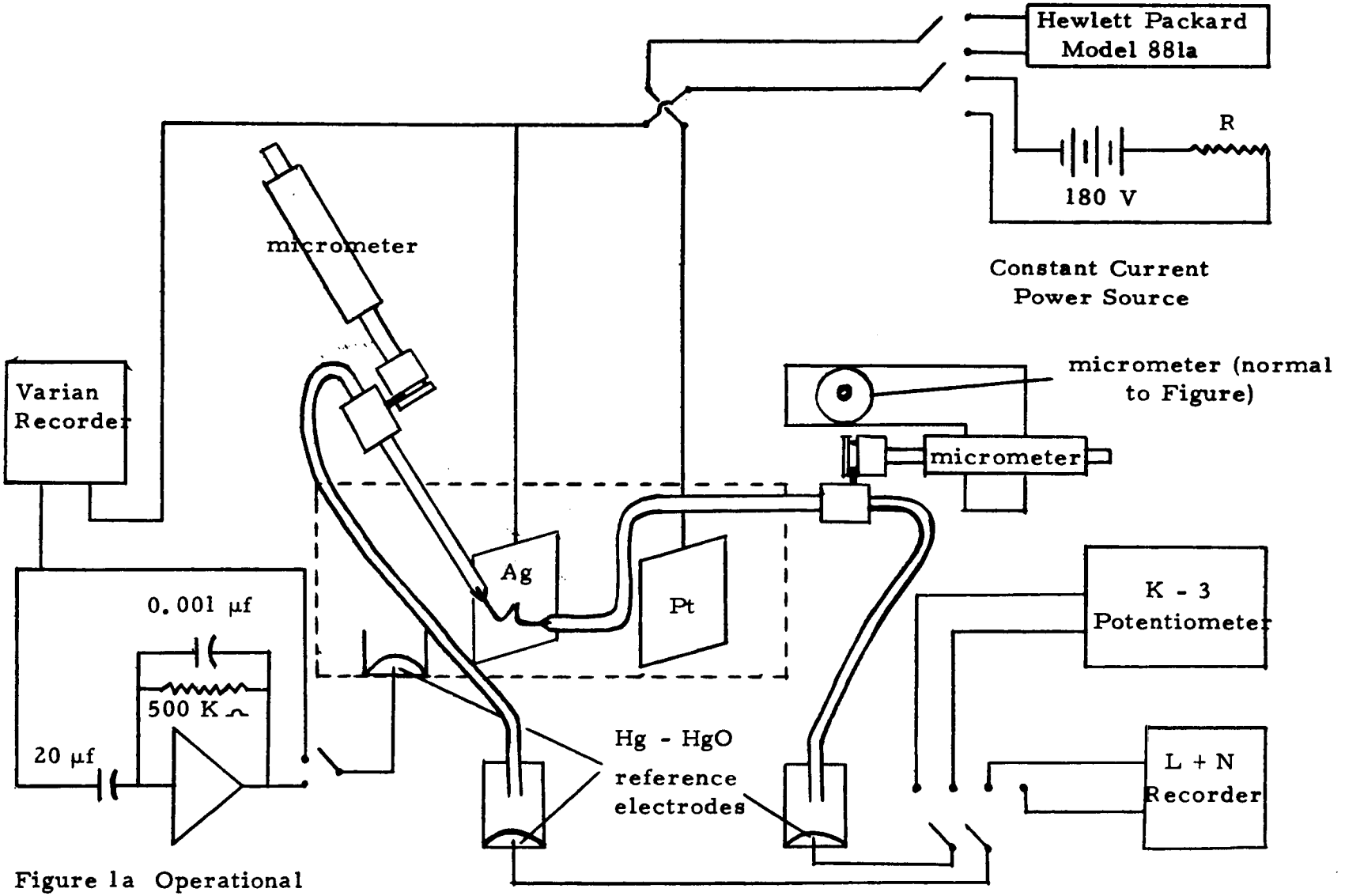


Figure 1a Operational amplifier as differentiator

Δ ∅ Measuring Circuit

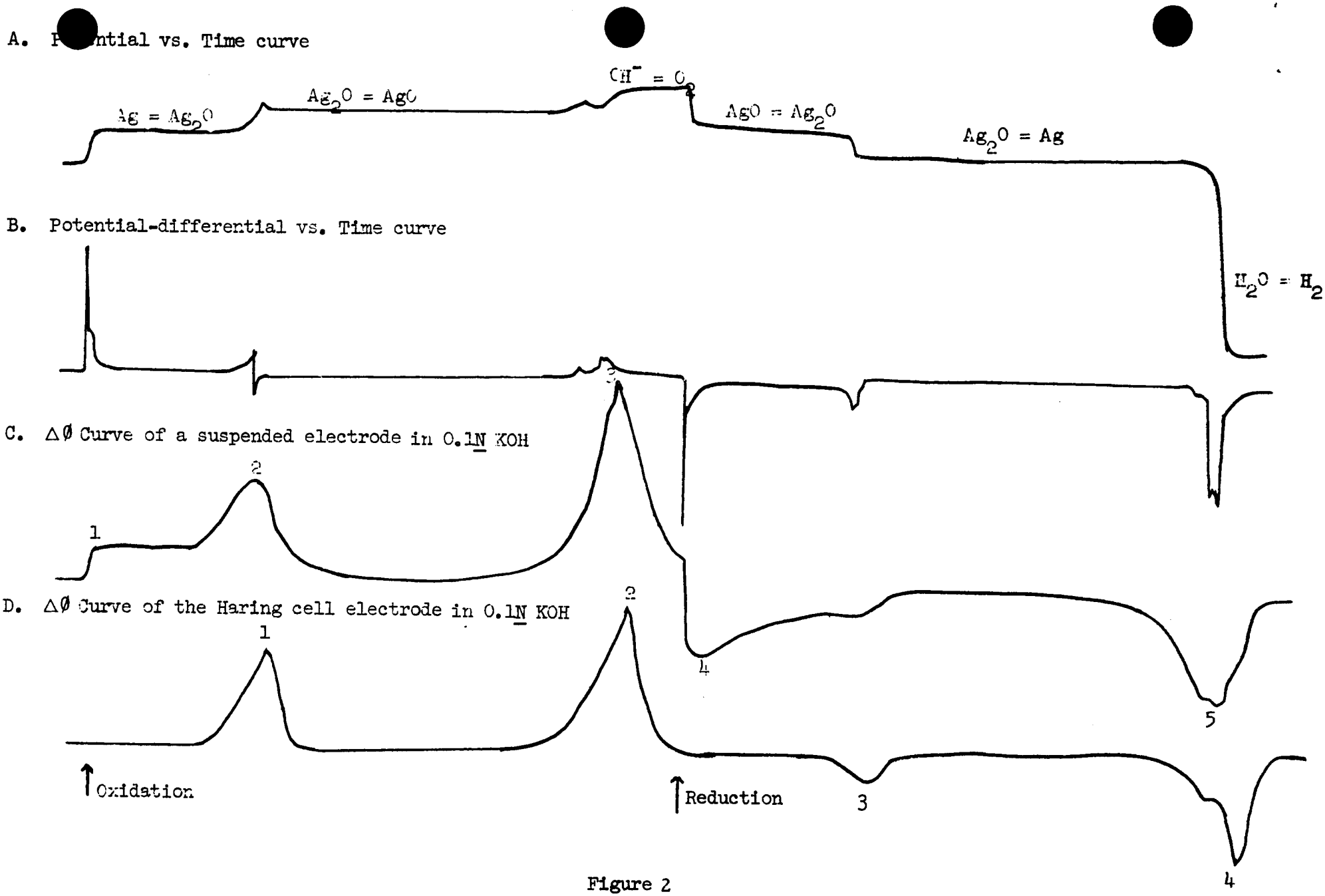


Figure 2

Simultaneous Runs

Curves A, B and C were made at the same time. Curve D was made separately with a simultaneous potential-time curve and then matched to curve A of this figure.

Figure 3

Comparison of three $\Delta\emptyset$ curves made during the oxidation of silver electrodes. (curves C and D also appear in Figure 2 )

C. $\Delta\emptyset$ Curve of a suspended electrode in 0.1N KOH

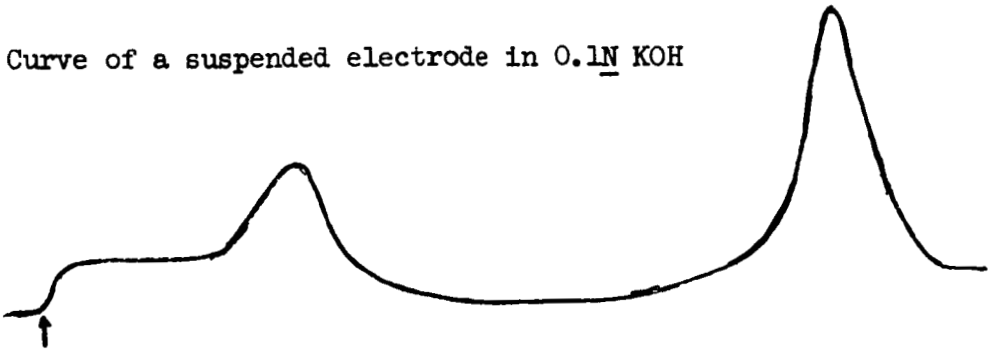

D. $\Delta\emptyset$ Curve of the Haring cell electrode in 0.1N KOH

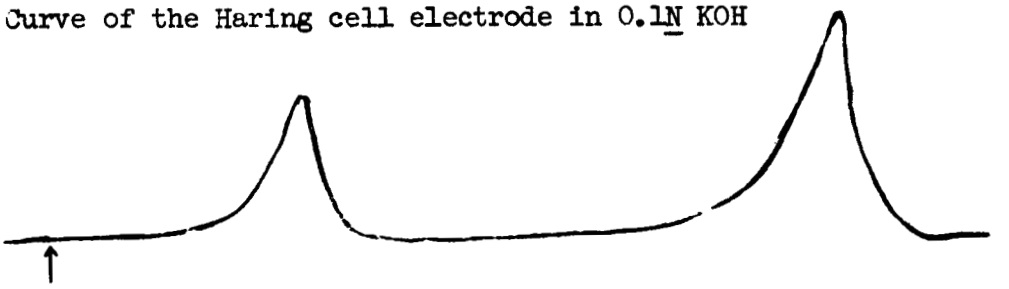

E. $\Delta\emptyset$ Curve of a suspended electrode in the ammoniacal electrolyte

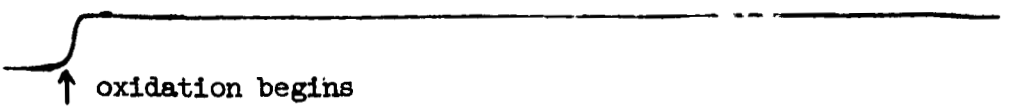

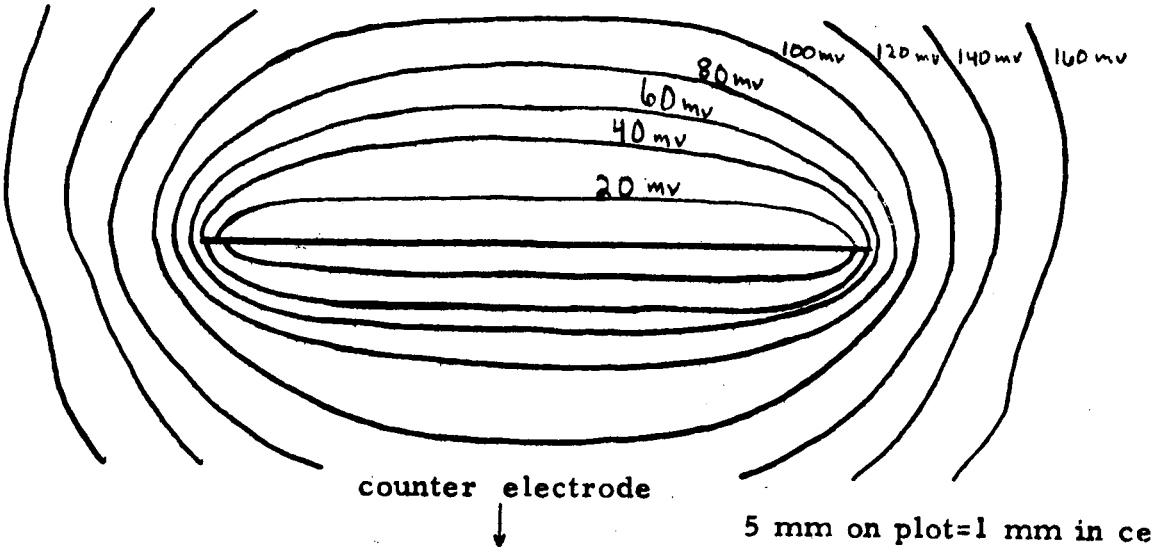


Figure 4 Equipotentials around a working suspended silver foil electrode

Figure 4a Diagram showing configuration of electrode used in Figure 4

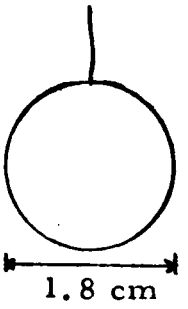


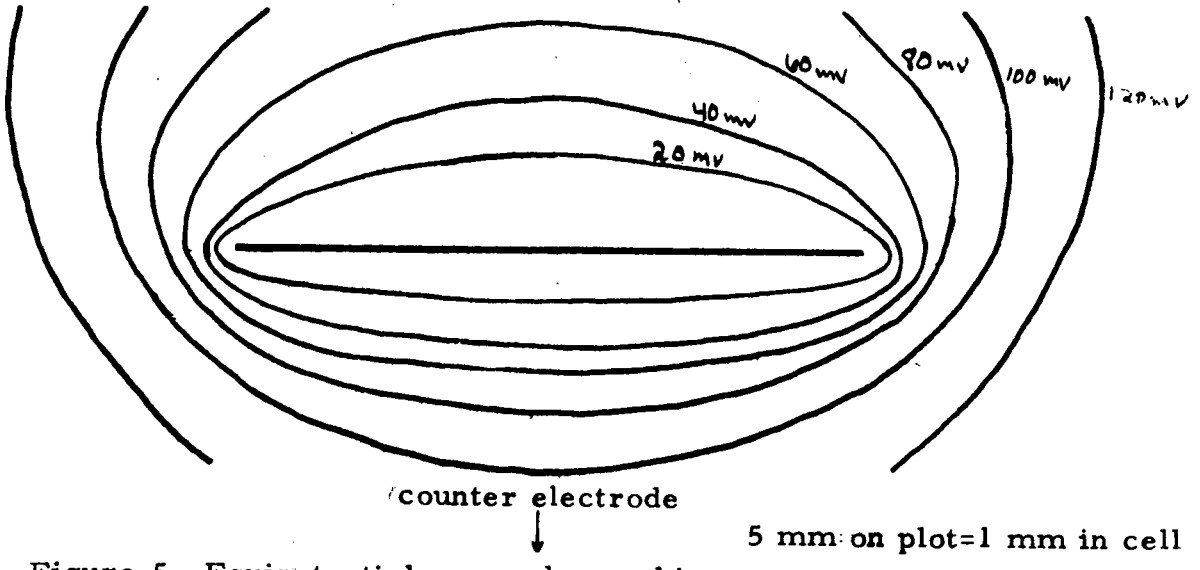


Figure 5 Equipotentials around a working suspended sintered silver electrode

Figure 5a Diagram showing configuration of electrode used in Figure 5

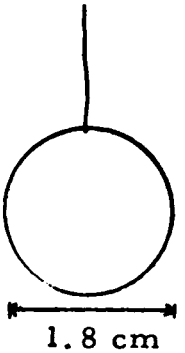

Figure 6 Equipotentials around a working suspended one-sided silver foil electrode

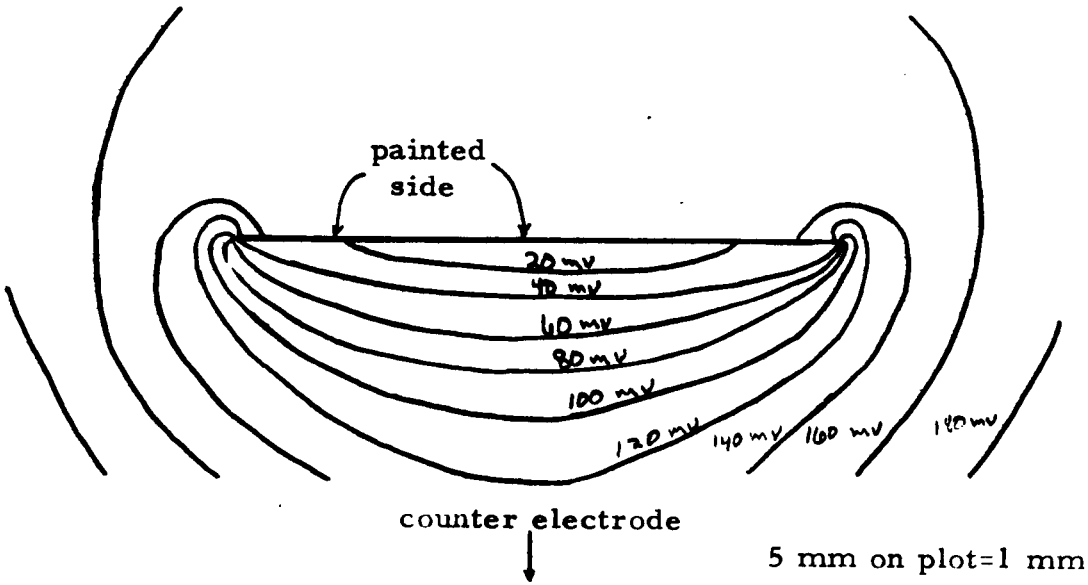


Figure 6a Diagram showing configuration of electrode used in Figure 6

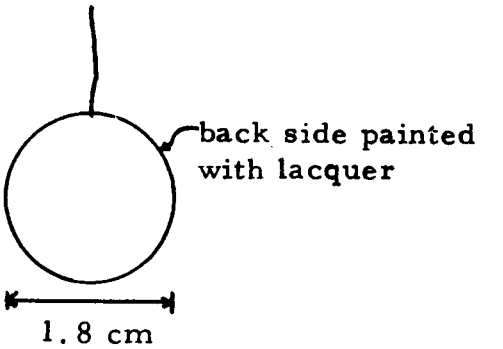

Figure 7 Equipotential map of electrode having configuration shown below

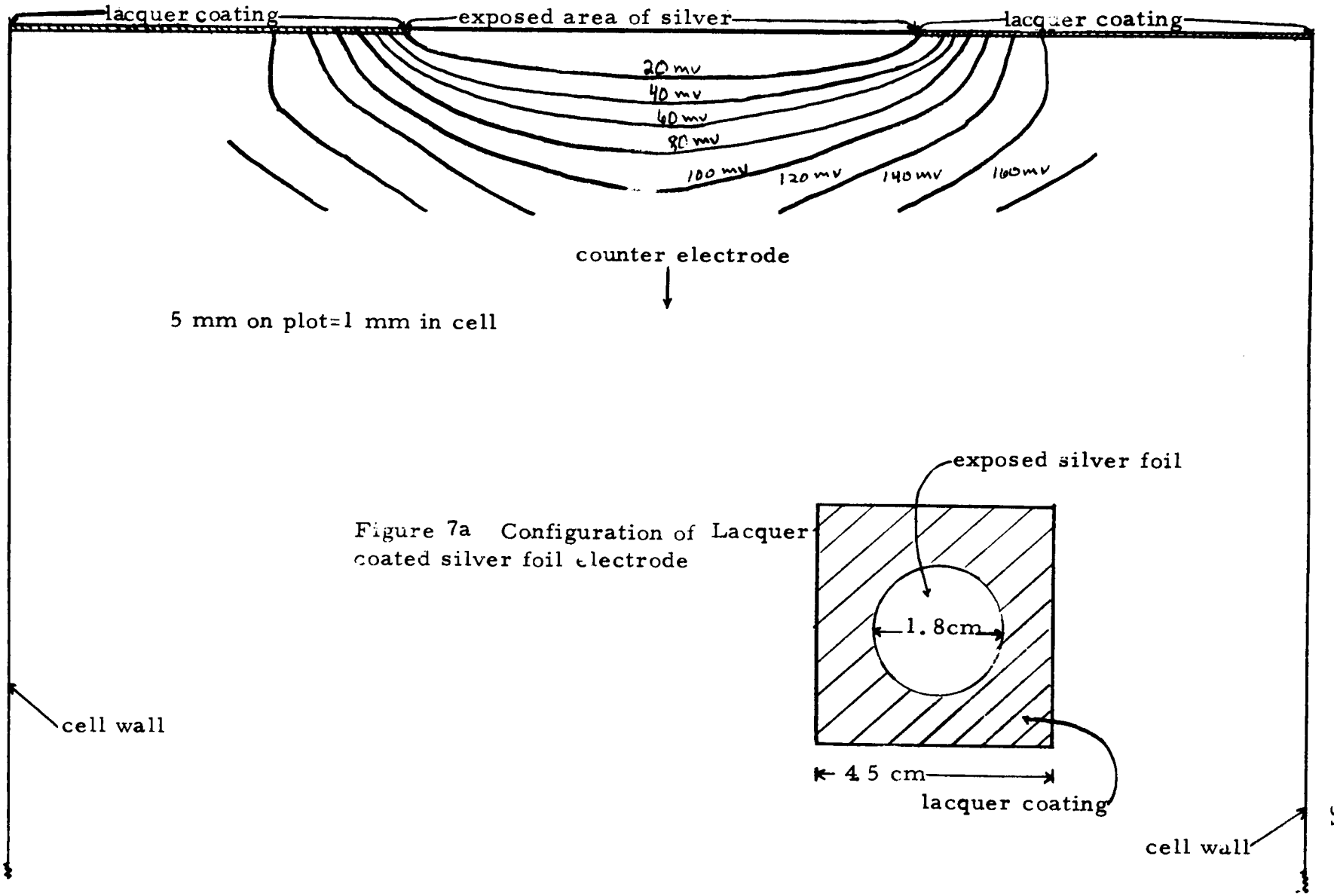





Figure 7a Configuration of Lacquer coated silver foil electrode

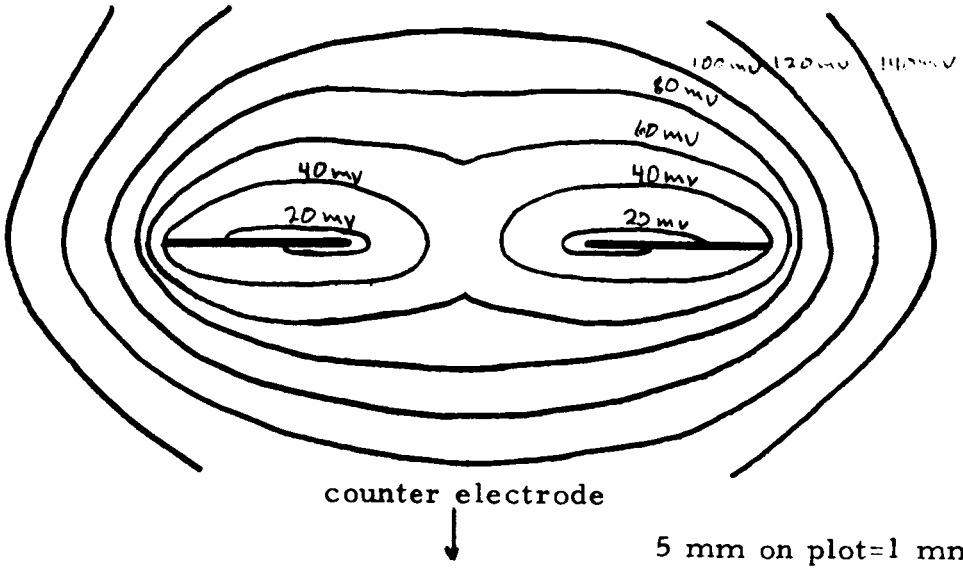


5 mm on plot=1 mm in cell

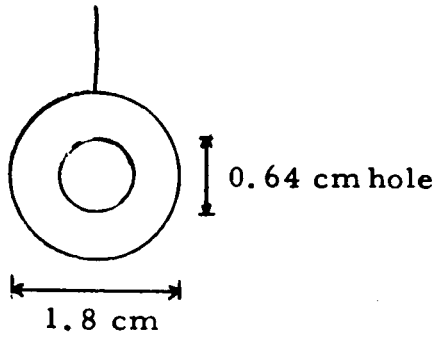


Figure 8 Equipotentials around a working suspended silver foil electrode with the center cut out

Figure 8a Diagram showing configuration of electrode used in Figure 8

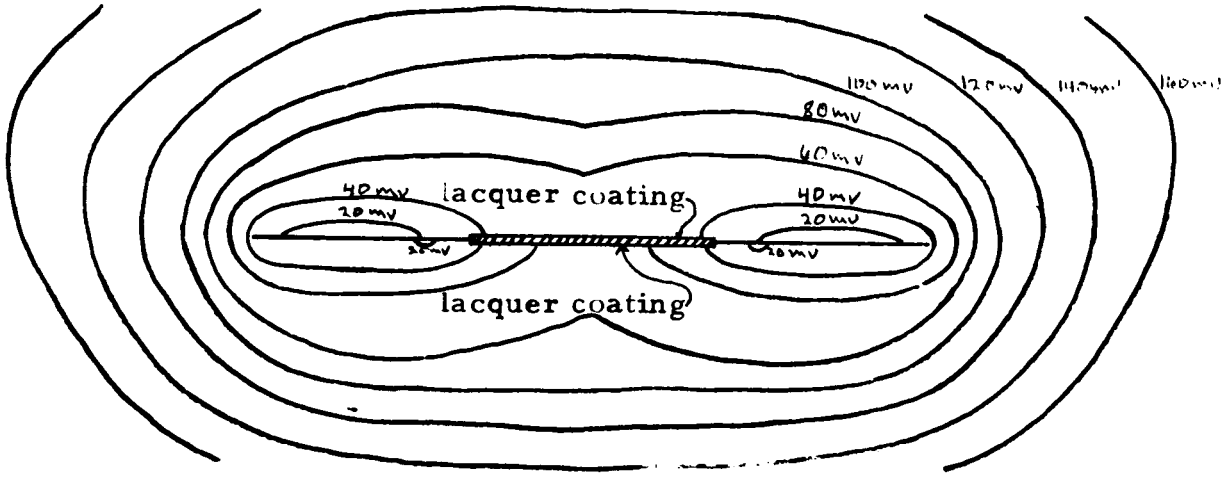


5 mm on plot=1 mm in cell

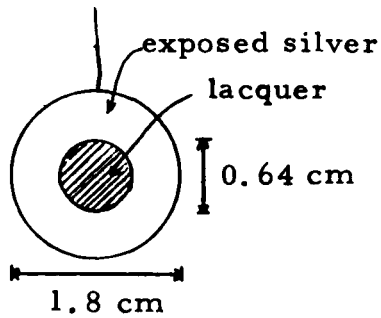


Figure 9 Equipotential map of a working suspended silver electrode with the center painted with lacquer

Figure 9a Diagram showing configuration of electrode used in Figure 9

Figure 10 Equipotential map of electrode having configuration shown below.

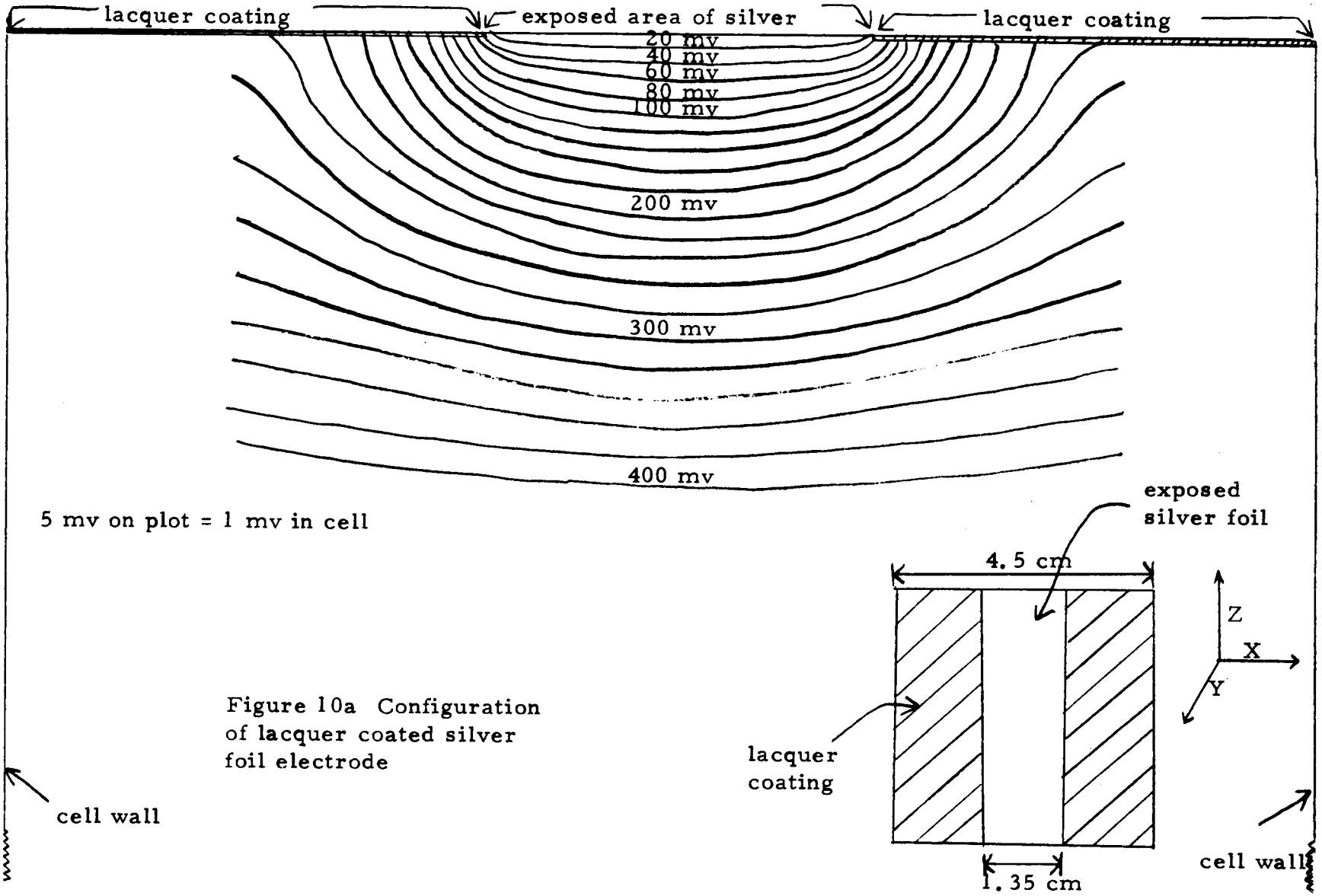


Figure 10a Configuration of lacquer coated silver foil electrode

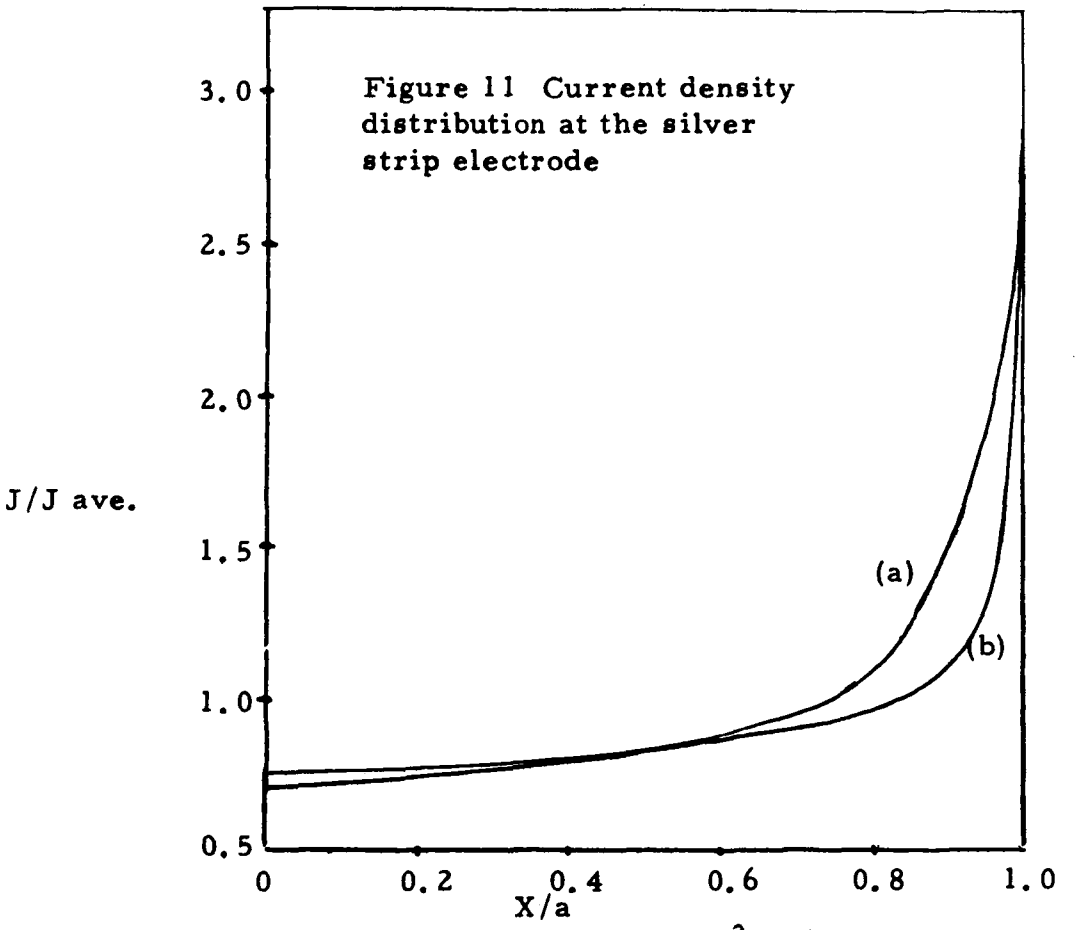


Figure 11 Current density distribution at the silver strip electrode

(a) From Wagner's analysis[3] (K/a = 0.10)

(b) From our data (K/a = 0.10)

X, is the distance from the electrode center and, a, is the half width of the electrode

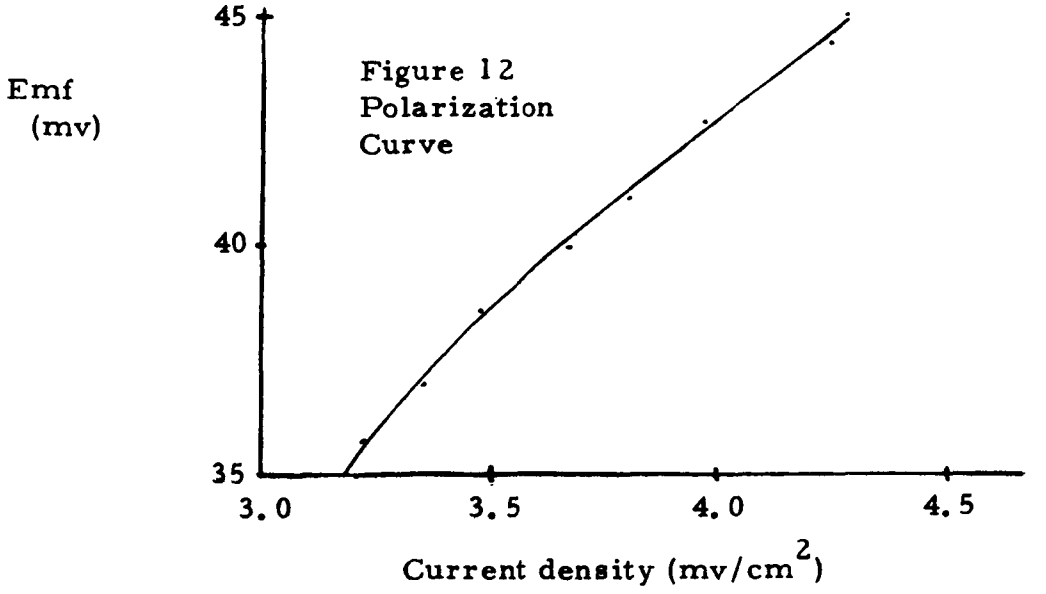


Figure 12 Polarization Curve

$$\frac{K}{a} = \frac{7.2 \times 0.00947}{1 \times .675} = 0.10$$

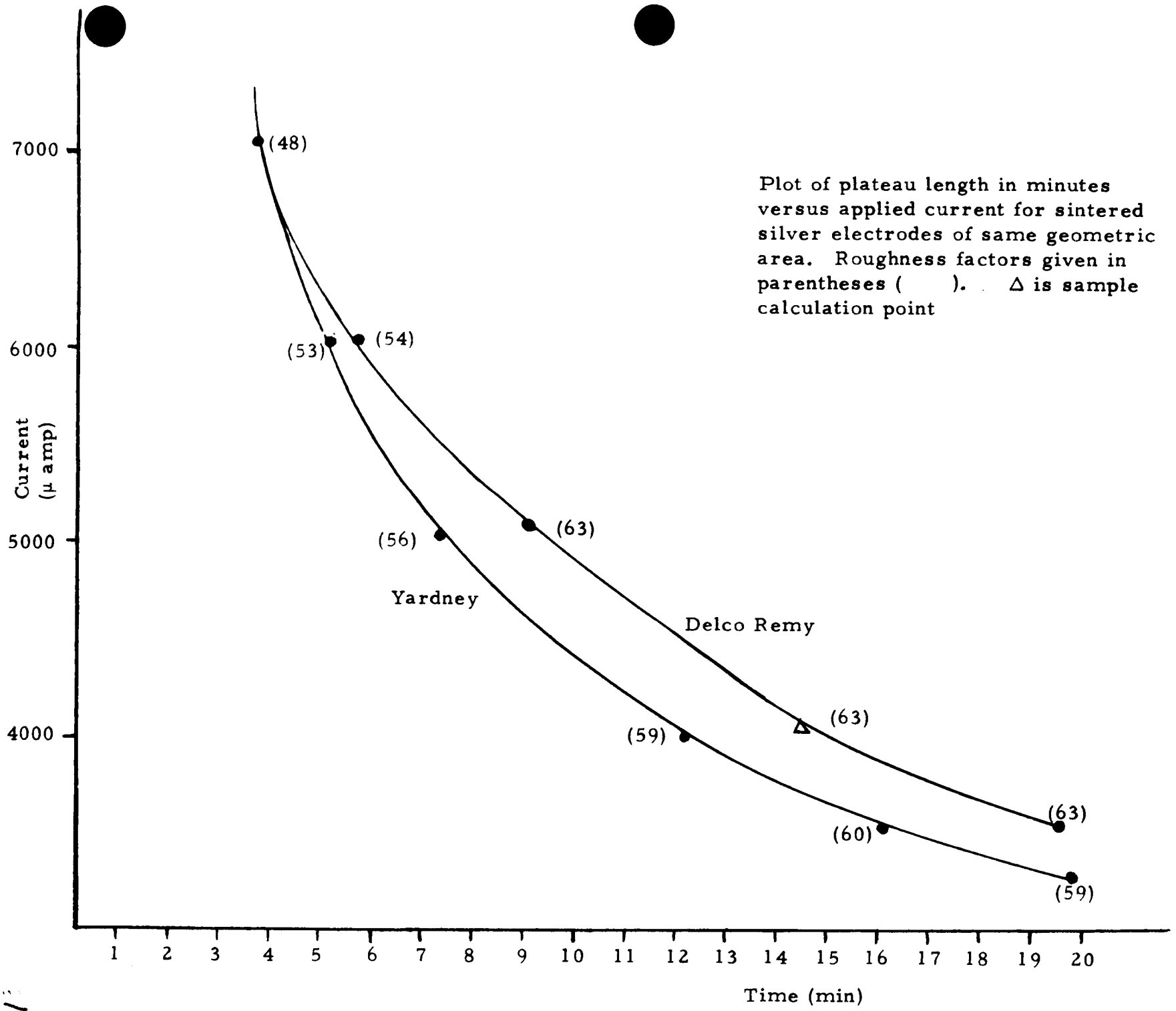
Plot of plateau length in minutes versus applied current for sintered silver electrodes of same geometric area. Roughness factors given in parentheses ( ). Δ is sample calculation point
7000
6000
5000
4000
Current (μ amp)
(48)
(53)
(54)
(56)
(63)
Yardney
Delco Remy
(63)
(59)
(60)
(63)
(59)
1 2 3 4 5 6 7 8 9 10 11 12 13 14 15 16 17 18 19 20
Time (min)

Figure 13

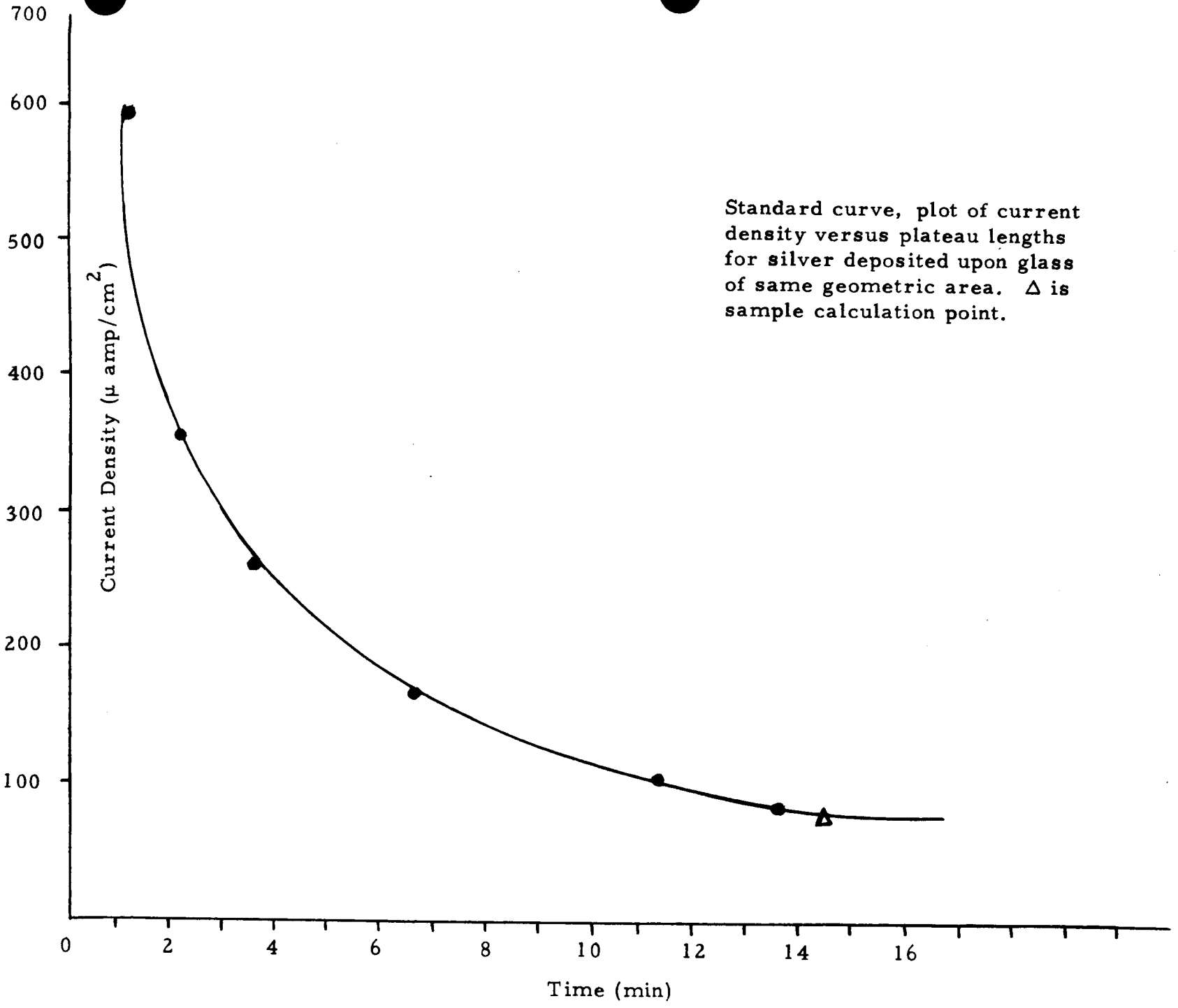


Standard curve, plot of current density versus plateau lengths for silver deposited upon glass of same geometric area. Δ is sample calculation point.

Figure 14

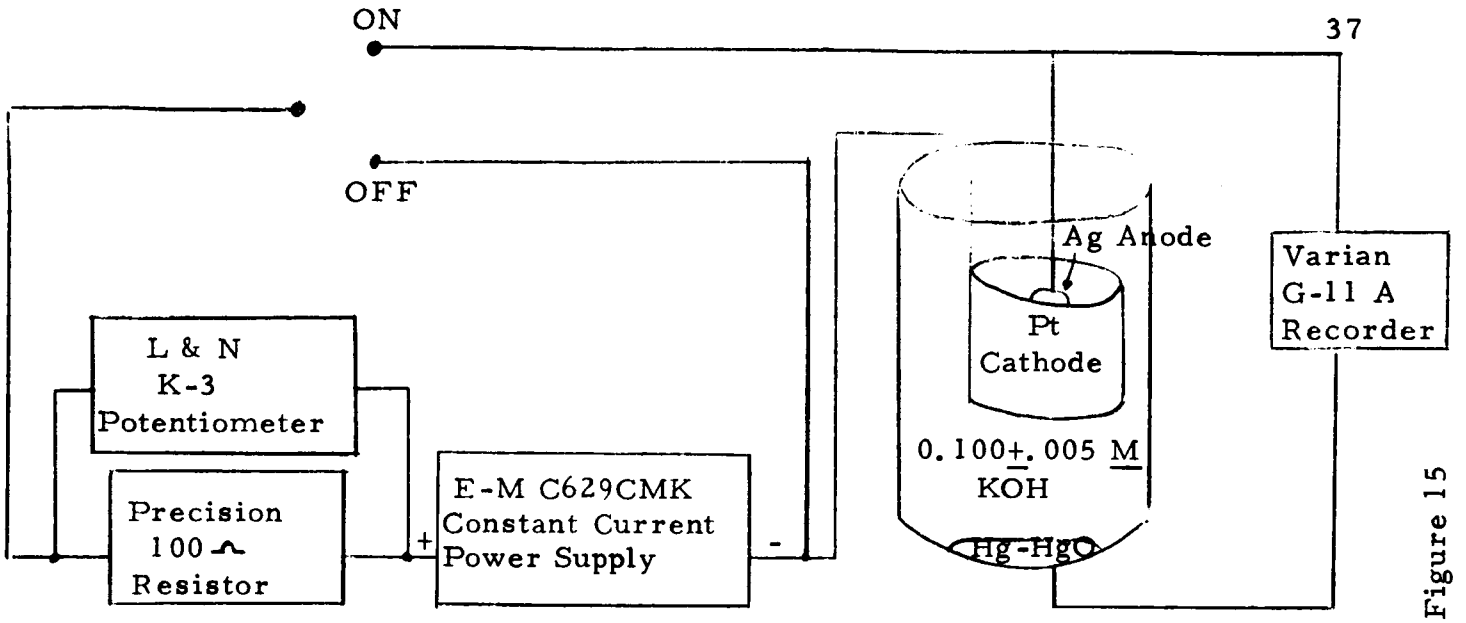


Figure 15

Detailed diagram of apparatus used in determining oxidation plateaus

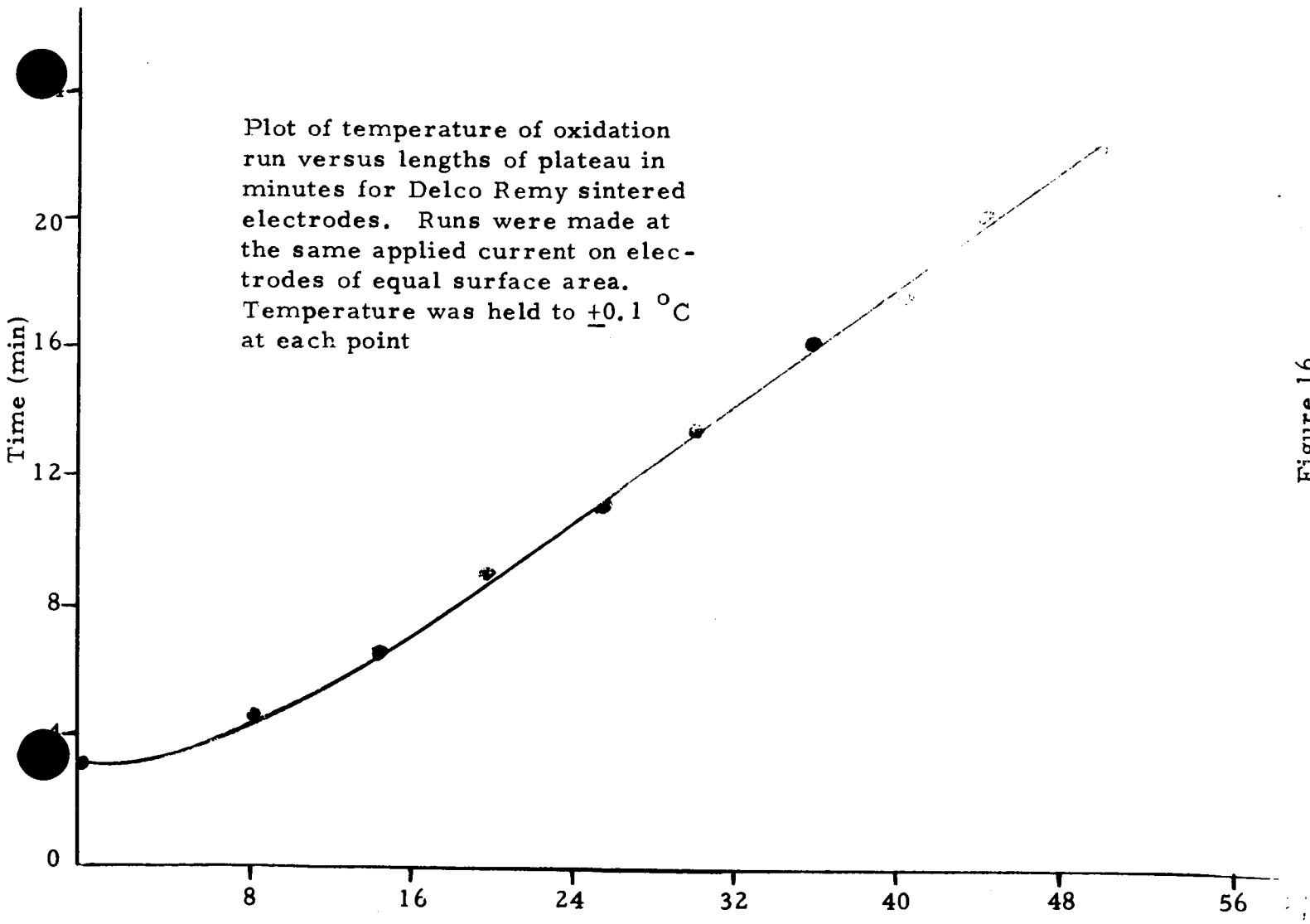


Figure 16

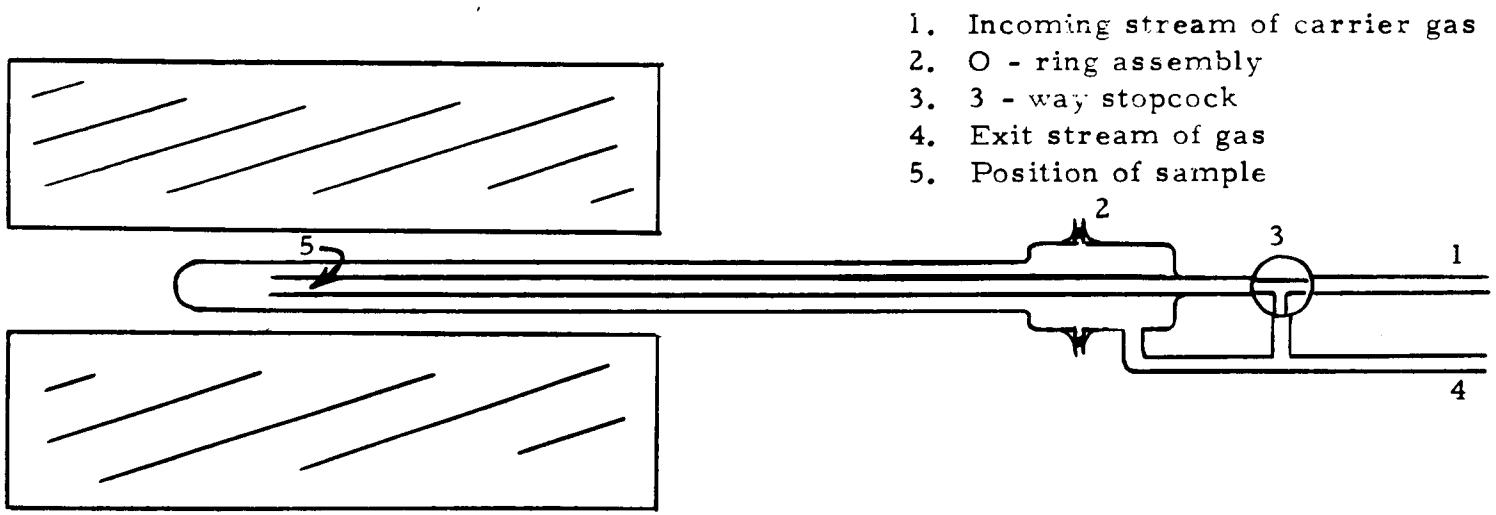


Figure 17 Pyrolysis Chamber

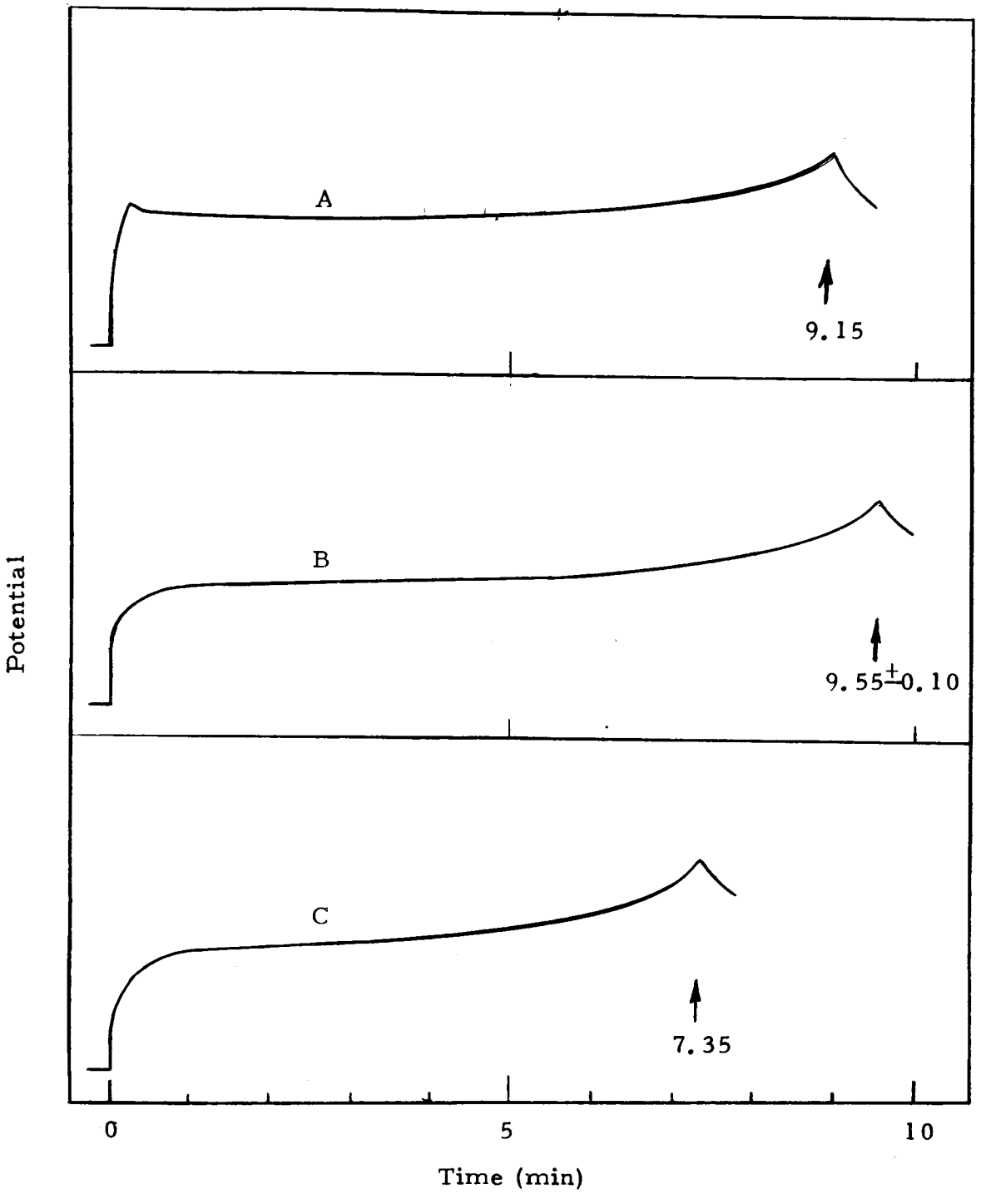


Figure 18 Electrolytic Oxidation at 28.2 °C of Pyrolyzed Sintered Silver Electrodes

A. Not Pyrolyzed
B. Pyrolyzed at 410 °C in $O_2$
C. Pyrolyzed at 625 °C in $O_2$

## REFERENCES


1. H. E. Haring, Trans. Electrochem. Soc., 49, 417, (1926).

2. C. Kasper, Trans. Electrochem. Soc., 77, 353 (1940).

3. C. Wagner, J. Electrochem. Soc., 93, 116, (1951).

4. I. Shain, Anal. Chem., 38, 1148, (1966).

5. G. L. Booman, W. B. Holbrook, Anal. Chem., 35, 1793, (1963).

6. J. A. Allen, Trans. Faraday Soc., 48, 273, (1952).

7. Allpress, Sanders, J. Catalysis, 3, 528-38, (1964).

8. R. L. Mass, Trans. Faraday Soc., 59, 216-29, (1963).

9. J. McCallum, J. E. Walling, and C. C. Faust, "Measurement of True Surface Area in Electrode," First Quarterly Technical Progress Report, Battelle Memorial Institute, Columbus, Ohio (undated).

10. (a) W. W. Porterfield and G. T. Miller, J. Electrochem. Soc., 113, 528, (1966).

    (b) T. P. Dirkse, F. De Haon, J. Electrochem. Soc., 106, 920-925, (1959).

11. (a) T. P. Dirkse, J. Electrochem. Soc., 106, 456, (1959).

    (b) T. P. Dirkse, F. De Haon, J. Electrochem. Soc., 105, 311, (1958).

12. G. H. Twigg, Proc. Roy. Soc. London A188, 92-104, (1964).

13. E. O. Fischer and H. Werner, "Metal $\pi$-Complexes," Elsevier, New York, (1966), p. 147.